Picophytoplankton lineages display clear niche partitioning but overall positive response to future ocean warming

Pedro Flombaum^{1,2,3}, Wei-Lei Wang¹, Francois Primeau¹, and Adam C. Martiny^{1,4,*}

¹Department of Earth System Science, University of California, Irvine, CA 92697, USA

²Centro de Investigaciones del Mar y la Atmósfera, CONICET, 1428 Buenos Aires, Argentina

10

5

³Universidad de Buenos Aires, Facultad de Ciencias Exactas y Naturales, Departamento de Ecología, Genética y Evolución,1428 Buenos Aires, Argentina

⁴Department of Ecology and Evolutionary Biology, University of California Irvine, CA 92697, USA

*Corresponding Author

University of California Irvine, 3208 Croul Hall, CA 92697, USA, Phone: 949-824-9713, Fax: 949-824-3874, amartiny@uci.edu

20

Keywords: Picoeukaryotic phytoplankton, Climate change, neural networks, niche models, biomass

Short title: Global present and future distributions of picophytoplankton

25

30

35

40

First Paragraph:

Earth System models predict a decline in ocean phytoplankton biomass^{1,2} due in large part to an expansion of ocean regions dominated by diverse picophytoplankton communities^{3,4}. Alternatively, you can predict future ocean phytoplankton biomass based on current abundances of diverse populations along environmental gradients using quantitative realized niche models⁵. Using a global dataset to calibrate a niche model, we project the global biogeography of the very abundant but little studied picoeukaryotic phytoplankton. We then combine this niche model with similar models for *Prochlorococcus* and *Synechococcus*⁶. We find that cell size differences between lineages parallel a latitudinal niche partitioning but a shared overall picophytoplankton biomass increase along a positive temperature gradient between 25°C and 30°C. Thus, future warmer ocean conditions can lead to elevated phytoplankton biomass in low latitude regions. Further biogeochemical model analyses suggest that future elevated upper-ocean nutrient recycling and lower nutrient requirements of phytoplankton can support increasing low latitude phytoplankton biomass. Such a previously unrecognized phytoplankton biomass response to climate change can have widespread ramifications for marine life in the ocean.

45 **Main:**

50

55

60

65

70

75

80

85

90

Earth System models are central to how we predict the impact of climate change on marine systems. Such models have primarily been designed for describing carbon and nutrient fluxes but are increasingly called upon for predicting ecosystem behavior including changes in the standing stock of ocean phytoplankton^{7,8}. However. phytoplankton biomass predictions are uncertain for at least two reasons. First, modelpredicted phytoplankton biomass are only cursorily calibrated by regional patterns in remotely sensed chlorophyll concentrations. However, the chl:C ratio can vary depending on phytoplankton diversity and physiology⁹ leading to high uncertainty in chlorophyllbased estimates of phytoplankton biomass¹⁰. Secondly, Earth System models utilize a simplified ecosystem based on few phytoplankton functional types¹¹. This approach is limited by requiring identifying and assigning a single set of growth parameters describing the physiology of a lineage¹² and fails to capture the high diversity known to exist within and across phytoplankton communities¹³. Thus, there is high uncertainty in existing estimates of biomass and the unknown role of phytoplankton diversity impedes our ability to reliably predict how biomass will respond to growing environmental changes^{6,10,12,14}.

High intraspecific diversity can enable the whole lineage to grow across broad environmental conditions leading to a wider fundamental niche than predicted from individual genotypes (Fig. S1)¹⁵. Thus, an alternative to Earth System models for predicting future changes to phytoplankton abundances is to establish realized niche models by quantifying abundances along existing ocean environmental gradients¹⁶. This approach is based on a simple tenet that the best estimate for future abundances is to find regions in the contemporary ocean with analogous environmental conditions (Fig. S1). A niche model lacks a mechanistic basis for the distribution of phytoplankton but implicitly 'embraces' the within lineage diversity, interactions between environmental factors, and poorly understood biotic effects of other organisms.

We previously applied a niche model approach to project how *Prochlorococcus* and *Synechococcus* will respond to future ocean conditions⁶. However, we are missing a key phytoplankton group with a substantial but unconstrained biomass: the globally distributed and highly diverse picoeukaryotic phytoplankton assemblage^{4,17,18}. Combined, these three groups constitute the picophytoplankton fraction and nearly all photosynthetic biomass in tropical and subtropical oligotrophic waters^{3,19}. Thus, future climate projections of total phytoplankton biomass in low latitude ocean regions must include picoeukaryotic phytoplankton.

Here, we used a global dataset to derive a neural network based niche model and asked what is the abundance and quantitative distribution of picoeukaryotic phytoplankton? We next combined this model with ones for *Prochlorococcus* and *Synechococcus* and asked how do environmental factors influence the abundance and niche partitioning among these lineages, and finally, how will total picophytoplankton biomass respond to future projected climate changes?

We estimated an annual globally integrated abundance of picoeukaryotic phytoplankton of 1.6 x 10^{26} ($\pm 1.8 \times 10^{25}$) cells. Using a neural network derived niche model trained on a geographically diverse dataset (Fig. S2 and Table S1), we were able to capture a substantial part of the global variability (Fig. S3, $R^2 = 0.46 \pm 0.01$). Regions of elevated concentrations (>10⁴ cells/ml) included an area above 45°N in the North Atlantic

Ocean, around the North Pacific Current, and a band near the southern subtropical convergence zone (Fig. 1). Picoeukaryotic phytoplankton were also projected in high abundances near upwelling zones including the eastern equatorial Pacific Ocean, the California Current, and the Benguela Upwelling zone. Lower abundances were predicted for the oligotrophic gyres and polar regions. We also observed seasonal changes with a globally integrated abundance minimum of 1.4×10^{26} ($\pm 1.1 \times 10^{25}$) cells and a maximum of 1.9×10^{26} ($\pm 6.8 \times 10^{24}$) cells in June and September, respectively (Fig. S4).

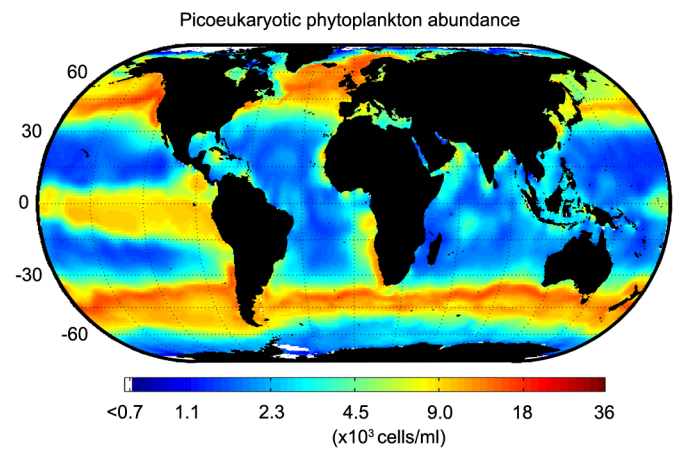


Figure 1. Global distribution picoeukaryotic phytoplankton abundance. Projected picoeukaryotic phytoplankton mean annual cell abundance at the sea surface as estimated by our niche model.

We next quantified the niche for picoeukaryotic phytoplankton along light (PAR), temperature, and nitrate gradients (Fig. 2). As expected for photosynthetic organisms, we observed a strong effect of light availability with the highest levels near the surface. There was an average increase in abundance by 1.4 orders of magnitude between surface and the deep euphotic zone light levels (Fig. 2A). In addition to light, there was a strong but non-linear relationship between temperature and cell density (Fig. 2B). The abundance was lowest (1.8 x 10³ cells/ml) at 0°C but increased to a maximum abundance (2.4 x 10⁴ cells/ml) at 8.5°C. Beyond the maximum, the abundance declined and reached a local minimum at ~21°C. Above this temperature, we saw an increase in cell numbers from 4 to 12 x 10³ cells/ml leading to intermediate concentrations in tropical waters. We also detected a non-linear correlation between nitrate availability and abundance (Fig. 2C). Low nitrate concentrations had little effect but we found a substantial increase peaking at 1.6 μ M of nitrate associated with a shift from 4 x 10³ to 1 x 10⁴ cells/ml. Above 1.6 µM, nitrate had a negative correlation to cell abundance reaching a minimum of 2 x 10³ cells/ml at high nitrate concentrations. This hump shaped distribution may be influenced by competition with *Prochlorococcus* and *Synechococcus* at the low end and larger phytoplankton at the high end of the nutrient gradient. The temperature or nitrate dependence of the predicted abundance did not change along gradients of the other variables suggesting limited interaction terms for these factors. However, the effect of PAR was less pronounced at lower temperatures (Fig. S5). In sum, picoeukaryotic phytoplankton displayed a clear global biogeography correlated with light, temperature, and nutrient availability.

120

95

100

105

110

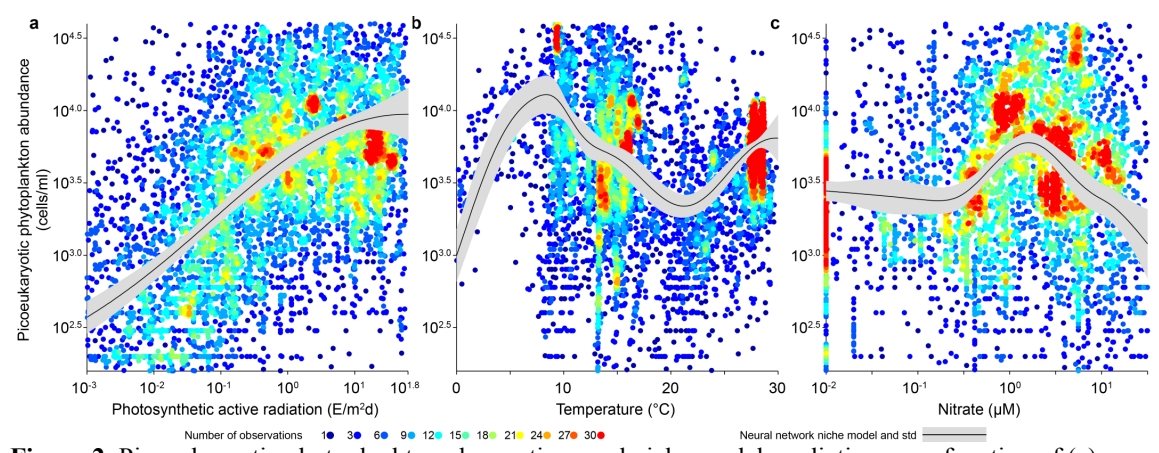


Figure 2. Picoeukaryotic phytoplankton observations and niche model predictions as a function of (a) photosynthetic active radiation (PAR), (b) temperature, and (c) nitrate. The line and shaded area represent the quantitative niche model output mean and standard deviation based on 100 trained neural networks. The niche model represents cell abundance at constant a) temperature and nitrate (15°C and 3.2 μ M), b) PAR and nitrate (1 E m⁻² d⁻¹ and 3.2 μ M), and c) PAR and temperature (1 E m⁻² d⁻¹ and 15°C). Symbol color represents number of overlapping observations in intervals of PAR 10^{0±1.2} E m⁻² d⁻¹ temperature 15±7.5°C, and nitrate 10^{0.5±1} μ M. See Fig. S4 for interactions between factors.

130

135

140

145

150

155

160

We observed clear niche partitioning along gradients of light and temperature among *Prochlorococcus*, *Synechococcus*, and picoeukaryotic phytoplankton (Fig. 3). The relative abundances of all lineages were generally positively influenced by increasing light levels (Fig. 3A). Prochlorococcus had an advantage at low light levels. In contrast, Synechococcus was strongly negatively related to declining light, whereas picoeukaryotic phytoplankton had an intermediate response. At high light levels, Synechococcus displayed maximum abundance. Prochlorococcus depressed abundances, and picoeukaryotic phytoplankton an intermediate response. Small eukaryotic phytoplankton like Ostreococcus strains show some light inhibition at elevated light levels (> 1.6 E m⁻² d⁻¹) but can still sustain intermediate growth rates^{20,21}. In contrast, individual *Prochlorococcus* strains can grow at very low light level but can be photoinhibited²². Further, some *Synechococcus* strains show limited light inhibition even at extremely high light levels but cannot sustain growth at low intensities²². Thus, the distribution along a light gradient is consistent with physiological studies of the three groups. Our models also revealed niche partitioning along a temperature gradient (Fig. 3B). The abundance of the largest sized group, picoeukaryotic phytoplankton, peaked at 8.5°C. The intermediate sized Synechococcus peaked at 10°C, whereas Prochlorococcus as the smallest was most common at high temperature. The separation in maxima along a temperature gradient corresponded negatively to cell size and thus support past regional studies¹⁸. The growth rate in all three lineages generally responds positively to temperatures in this range, which should lead to a positive relationship between abundance and temperature ^{22,23}. However, the decline in picoeukaryotic phytoplankton and *Synechococcus* at intermediate temperatures and the sharp decline in abundance of *Prochlorococcus* below 20°C could be the outcome of competition with other phytoplankton linages. We then combined the three models to predict changes in total picophytoplankton carbon biomass with temperature (Fig. 3C). Changes in picoeukaryotic phytoplankton controlled the cumulative biomass below ~20°C, whereas especially changes in *Prochlorococcus*

abundance was important above this threshold. As such, total picophytoplankton biomass increased with temperature above $\sim 20^{\circ}$ C.

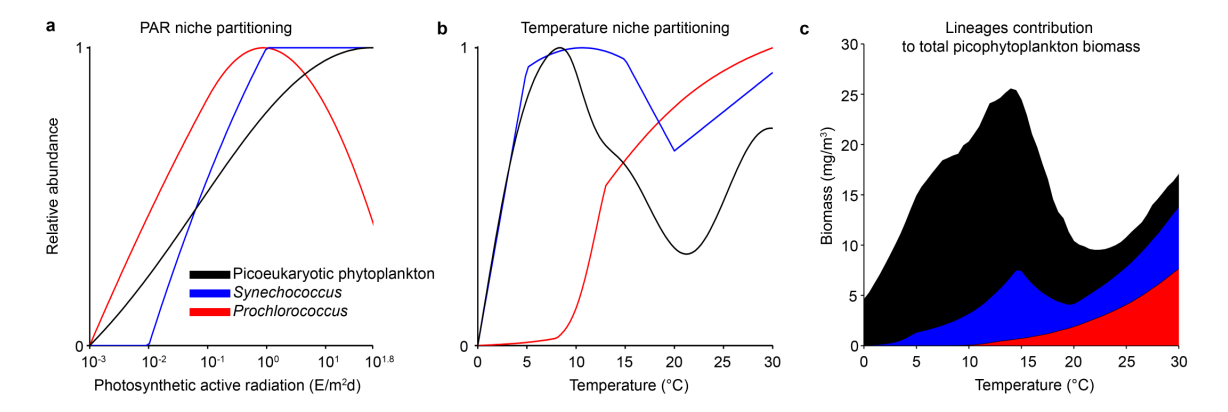


Figure 3. Niche partitioning among picoeukaryotic phytoplankton, *Synechococcus*, and *Prochlorococcus*. Predicted cell abundance relative to the difference between minimum and maximum cells/ml as a function of (a) photosynthetic active radiation (PAR) at constant temperature and nitrate concentration and (b) temperature at constant light and nitrate concentration. (c) Contribution of picoeukaryotic phytoplankton, *Synechococcus*, and *Prochlorococcus* to total picophytoplankton biomass as a function of temperature.

165

170

175

180

185

190

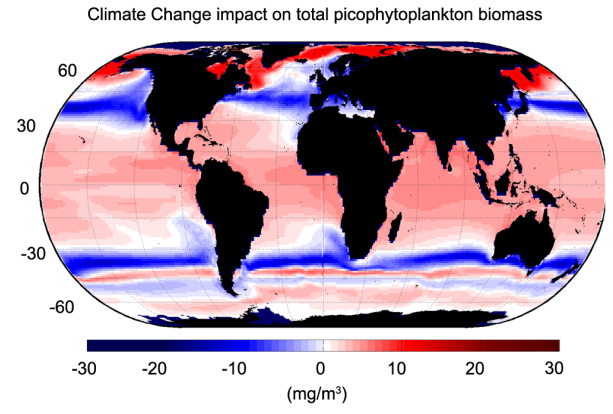
195

We next quantified the total picophytoplankton carbon biomass in the global ocean as well as the contribution by each lineage. The combined mean annual picophytoplankton biomass was 0.55 ± 0.03 Pg C in the global ocean, and thus higher than most biogeochemical model estimations¹¹, but smaller than earlier projections²⁴. Picoeukaryotic phytoplankton, *Synechococcus*, and *Prochlorococcus* each contributed 45%, 27%, and 27% of total picophytoplankton carbon biomass, respectively. The niche partitioning of each lineage along a temperature gradient translated into clear regional differences in their contribution to surface carbon biomass (Fig. 3C and Fig. S6A-C). Picoeukaryotic phytoplankton dominated picophytoplankton biomass at high latitudes and upwelling regions (Fig. S6A). At lower latitudes, Cyanobacteria were more common with *Prochlorococcus* contributing slightly higher biomass proportions than *Synechococcus* (Fig. S6B-C). The combined picophytoplankton biomass varied between ~5 mg C/m³ in the oligotrophic gyres to ~25 mg C/m³ in temperate regions with high picoeukaryotic phytoplankton abundances (Fig. S6D).

We compared our biomass estimations against an Earth System model (GFDL ESM2) prediction for the current ocean. Picophytoplankton constituted 53% of global ocean surface phytoplankton biomass and were generally equal to (or slightly above) a global community ecosystem model estimate of total phytoplankton biomass in most regions between 60°N and 60°S (Fig. S6E)³. As expected, picophytoplankton contributed less to overall biomass in polar regions and some upwelling zones, where larger phytoplankton lineages proliferate. Our biomass estimate was up to 50% higher than past model assessments in some regions including warm parts of the oligotrophic gyres (e.g., the Western Pacific Warm Pool). Thus, there was substantial discrepancy between our estimated picophytoplankton biomass levels and the GFDL ESM2 global model predictions.

Finally, we combined niche models with estimates of future ocean conditions to predict how total picophytoplankton biomass could respond to climate change.

200 Picophytoplankton biomass was sensitive to projected ocean environmental changes and showed a global increase of 0.05 ± 0.02 Pg C under the high emission RCP8.5 scenario. Mean surface biomass between 30°N and 30°S was 12 ± 2.4 and 15 ± 1.9 mg/m³ for the historic and RCP8.5 scenario (Fig. 4 and Fig. S7). However, there were big regional differences leading to places with strong declines (primarily upwelling regions and a 205 temperate band around 40°) or increases (e.g., tropical Indian Ocean). The change in total picophytoplankton biomass was driven by parallel biomass increases of *Synechococcus* and *Prochlorococcus* between 20°C and 30°C, whereas integrated picoeukaryotic phytoplankton biomass stayed flat (Fig. 3C). As total picophytoplankton constitute nearly all biomass in oligotrophic regions^{3,19}, we can use the combined niche models as an initial estimate for how low latitude total phytoplankton biomass will respond to 210 environmental changes. Thus, our projection suggests elevated picophytoplankton and likely total phytoplankton biomass in most low latitude regions in response to projected future climate changes (Fig. 4).



215

220

225

230

235

Figure 4. Projected impact of climate change on total picophytoplankton carbon biomass. Difference in surface total picophytoplankton carbon biomass estimated for the end of 21st and 20th centuries based on temperature and nitrate concentration simulated under the RCP8.5 and historic CMIP5 scenarios.

Phytoplankton biomass in low latitude regions is traditionally thought to be negatively controlled by stratification and associated nutrient supply¹. We have three separate hypotheses for how ocean warming would elevate low-latitude surface biomass independently of the vertical nutrient supply. First, small particles may be exported less efficiently and organic material is respired faster at high temperature²⁵. As seen for particulate iron²⁶, the combined effect will result in a temperature dependent upper ocean nutrient retention. Such a nutrient retention effect can be illustrated with a simple box model (Fig. S8). Here, the phytoplankton biomass in the surface ocean is augmented when biomass export is less efficient and nutrients are recycled faster. Secondly, access to the large stock of organically bound nutrients (e.g., DOP) in oligotrophic waters may be more accessible at elevated temperatures²⁷. Thirdly, 'frugal' phytoplankton can increase cellular C:N or C:P by >50% in warm, nutrient deplete environments^{28,29}. We incorporated the three hypotheses into an global biogeochemical model (Fig. 5 and Fig. S9). The simulations backed that some combination of modest increases in upper ocean nutrient retention and the elemental composition of phytoplankton can support elevated surface biomass across low latitude regions independently of the vertical nutrient supply strength. In contrast, increases in the remineralization of DOP only led to small changes

in surface phytoplankton biomass. Thus, phytoplankton biomass may increase in the absence of any 'new' nutrients in low latitude regions and are sensitive to other temperature-driven ecosystem processes.

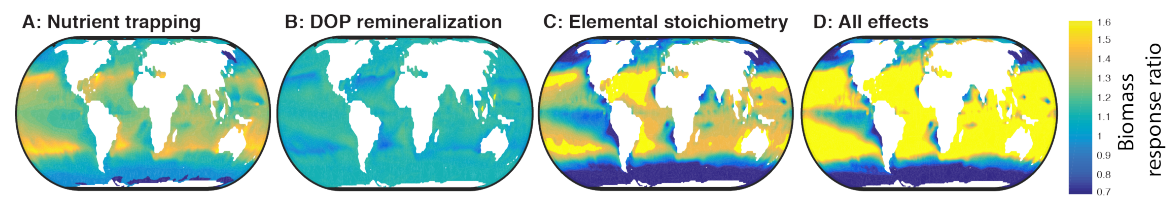


Figure 5. Evaluation of ecosystem regulation mechanisms on phytoplankton biomass. Impact of increased nutrient retention, DOP remineralization, elemental stoichiometry, and the combined effect for the top 35 m ocean biomass.

This work presents divergent future predictions for low-latitude phytoplankton in a warming world. Earth System models predict a decline whereas our new niche models predict an increase in biomass. However, both approaches are associated with significant uncertainty. Biomass estimates in Earth System models are generally calibrated against chlorophyll despite known variations in chl:C and use a simplified ecosystem description. Niche models assume phytoplankton biomass will share the same relationship to environmental parameters today and in the future and do not include impacts of other factors like pH or predation. These uncertainties and the strongly divergent outcomes of the two approaches call into question the generally accepted prediction of future declines in low-latitude phytoplankton biomass. Before confident predictions can be made, the potential impacts of other feedbacks such as efficient recycling of nutrients by diverse communities or phytoplankton with high C:nutrient biomass composition must be evaluated. Thus, our analyses indicate that a previously uncharacterized positive response in total phytoplankton biomass to warming in low latitude environments may be important to future ocean biology and ecosystem functioning.

Methods:

240

245

250

255

260

265

270

275

Dataset. All analyses were done using Matlab (Mathworks, MA). We obtained 13,771 picoeukaryotic phytoplankton observations from available public repositories and primary sources of a total of 39 cruises and time series covering major ocean regions and diverse environments (Fig. S2 and Table S1). Picoeukaryotic phytoplankton are defined as red fluorescent cells larger than *Prochlorococcus* and less than 2-3 μm in cell diameter. We only considered cell counts by flow cytometry. Samples covered a latitudinal range from 71.4°N to 66.1°S up to 400 m depth. Ancillary temperature and nitrate records were available for all but 2,334 and 6,530 observations, respectively, which we complemented with 1° monthly depth-dependent averages from the World Ocean Atlas (www.nodc.noaa.gov). To avoid analytical issues with detection limits, we imposed a minimum nitrate concentration of 0.01 μM. We calculated surface PAR (8 d averaged, 0.047° grid cell) using SeaWiFS and MODIS observations. Downward PAR was estimated using the attenuation coefficient K_{490} from SeaWiFS and MODIS (http://oceancolor.gsfc.nasa.gov) and corrected for chlorophyll a^{31} , and a minimum of 10^{-3} E/m²d was imposed.

Neural network analysis. To partition the non-linear relationship and interactions 280 between oceanographic factors and predict the overall distribution of picoeukaryotic phytoplankton, we trained a feed-forward back-propagation neural network with 10 nodes and up to 1000 epochs⁶. We evaluated the inclusion of temperature, PAR (log₁₀ transformed), and nitrate concentration (log₁₀ transformed) and found that all three factors contributed to describing log-transformed abundances of picoeukaryotic 285 phytoplankton. We used 50% of the observations for training (selected randomly) and the rest for validation. Optimization of the network was evaluated using Bayesian regularization. This process was repeated 100 times to estimate the variance in quantification. We then identified the contribution and interactions of environmental factor by sequentially varying each factor between the minimum and maximum observed 290 value (100 steps). This was repeated across all 100 trained networks to assess any bias associated with the data selection and the variation across the ensemble is the reported variance. Any bias regarding differences in cruises or in regional effects were not detected⁶.

295 **Biomass contribution.** To estimate global cell abundance of picoeukaryotic phytoplankton, we used as input to our neural network models monthly average temperatures and nitrate from the World Ocean Atlas 2005 (1°x1° resolution), and PAR and K₄₉₀ values derived from satellite data (SeaWiFS 0.083°x0.083°) and obtained predicted abundances for each set of conditions. We estimated annual globally integrated 300 cell abundance by integrating monthly cell abundance from surface to 205 m deep (in layers of 10 m) and a 1°x1° resolution grid. We estimated the annual globally integrated cell abundance standard deviation using the 100 trained neural networks. For sea surface abundance, we used the first layer. As the neural network analysis was done in log₁₀ space, we back-transformed cell abundances using a correction of 1.84 (the ratio of the 305 mean in regular space against the lognormal mean). Cell abundance for *Prochlorococcus*, and Synechococcus were estimated using existing quantitative niche models based on temperature and PAR⁶. We converted cell abundances to biomass using reported cellular carbon biomass content estimates for *Prochlorococcus* (50 fg C/cell), *Synechococcus* (175 fg C/cell), and picoeukaryotic phytoplankton (1500 fg C/cell)³². Total 310 picophytoplankton biomass was the sum of the three lineages. For total phytoplankton biomass, we reported values simulated by the GFDL ESM2 Earth System model³³.

Future predictions. To evaluate the effects of future climate change on picoeukaryotic phytoplankton abundance and biomass, we used as input to our neural network models year values of temperature and nitrate outputs from Earth System models under the Representative Concentration Pathway 8.5 (RCP8.5 – equivalent to a radiative forcing of 8.5 W m⁻² in 2100) and Historical scenarios. Light fields were identical across simulations. We calculated the effect of climate change for each lineage and total picophytoplankton biomass as the difference between 2070-2099 and 1970-1999 for the RCP8.5 and historical scenarios. We imposed a maximum sea surface temperature of 30°C as model predictions of higher temperature are uncertain due to poorly constrained atmospheric convection feedbacks. The combination of temperature and nitrate in climate model projections for the end of the century were well represented in our observation dataset, and no extrapolation was necessary (Fig. S10). We used an ensemble of eight

315

Earth System models, CanESM2, CESM1 BGC, GFDL ESM2G, HadGEM2 ES, IPSL CM5A MR, MIROC ESM, MPI, and NorESM1 ME³⁴ to estimate mean and standard deviation values for present and future projections. Standard deviation for climate change projection was estimated for the multi-model ensemble. It is important to note that we assume limited additional feedback between the predicted changes in phytoplankton abundances and nitrate concentration (i.e., beyond what is already captured by the climate model).

Our predictions are based on some important assumptions. First, we assume perfect lineage niche conservatism³⁵ as the very large population size of lineages suggests selection among existing ecotypes rather than *de novo* mutations will likely be more common. Secondly, it is assumed that other abiotic as well as biotic interactions like predation or competition with other lineages track the applied underlying environmental conditions. This may be a reasonable assumption to a first order as larger competing phytoplankton as well as grazers and viruses putatively are sensitive to the same underlying environmental ranges. Thirdly, climate change may lead to environmental conditions not currently present in the ocean (e.g., low pH) leading to changes in niches and future abundances not captured by our analysis.

Box model design for evaluating the impact of nutrient retention by phytoplankton in the euphotic layer. We developed a simple model to illustrate the effect of nutrient 345 recycling and retention by phytoplankton in the euphotic layer (Fig. S8). In particular, we wanted to demonstrate that the standing stock of phytoplankton is sensitive to the degree of nutrient recycling and retention. The model captures the major physical and biological processes controlling nutrient cycling in the upper ocean in terms of two prognostic variables: P the living pool of nutrients in phytoplankton, and N the dead pool of 350 dissolved nutrients. Nutrients from the dead pool are taken up by phytoplankton in the upper ocean at a rate uPN and returned to the dead pool at a rate kP. The model includes a loss of nutrients by sinking particles at a rate sP, which is balanced by a net return flux $q(N_d - N)$, where N_d is the nutrient concentration in the deep ocean, which is assumed constant, and q the water-mass exchange rate between the deep and upper ocean. The 355 differential equations governing the above processes are

$$\frac{dN}{dt} = qN_d + kP - qN - uNP,\tag{1}$$

and

360

335

340

$$\frac{dP}{dt} = -(q+k+s)P + uNP. \tag{2}$$

These equations can be re-expressed in non-dimensional form

$$\frac{dn}{d\tau} = 1 + rp - n - \gamma np$$

$$\frac{dp}{d\tau} = -p - rp - \epsilon p + \gamma np, (3)$$

in which we have rescaled the dependent and independent variables by N_d and q respectively

$$n = \frac{N}{N_d}$$
 , $p = \frac{P}{N_d}$, $\tau = qt$, (4)

and introduced the following dimensionless parameters

$$\gamma \equiv \frac{u}{q} N_d , \quad r \equiv \frac{k}{q} , \quad \epsilon \equiv \frac{s}{q}$$
 (5)

The steady-state solution, obtained by setting the time derivatives to zero, is given by

$$n_{ss} = \frac{1+r+\epsilon}{\gamma},$$

$$p_{ss} = \frac{1}{1+\epsilon} \left(1 - \frac{1+r+\epsilon}{\gamma} \right). \tag{6}$$

375

380

To simplify the above expression, we consider parameter values appropriate for low latitude ecosystems where picophytoplankton dominates. For the subtropical gyre, we can assume that the rate of nutrient uptake is much faster than the vertical supply rate so that $\gamma \gg 1$. Two limits are of interest. The first, $\epsilon \gg 1$, corresponding to fast sinking phytoplankton leading to a low standing stock of biomass in the upper ocean:

$$p_{ss} \approx \epsilon^{-1}$$
. (7)

385 The second, $\epsilon \ll 1$, corresponding to more slowly sinking small phytoplankton, leads to a large stock of biomass in the upper ocean

$$p_{ss} \approx 1 - \epsilon$$
. (8)

Both solutions are independent of the nutrient supply rate and illustrates that the system can achieve different levels of biomass regardless of the nutrient supply rate. Instead, the biomass level can depend on the efficiency with which nutrients are retained in the upper ocean. A low retention efficiency corresponding to particulate sinking rates that are fast compared to the supply rate ($\epsilon \gg 1$) leads to a low biomass $P \approx \frac{q}{s} N_d$. Conversely, a high retention efficiency corresponding to particulate sinking rates that are slow

compared to the supply rate ($\epsilon \ll 1$) leads to a high biomass $P \approx N_d \left(1 - \frac{s}{q}\right)$.

Design of the ocean biogeochemical model. We wanted to test possible alternatives to nutrient supply that can result in an increase in biomass under future climate conditions within a 3-D ocean circulation model. Our model reproduced the transport and cycling of three pools of P, dissolved inorganic P (DIP), dissolved organic P (DOP), and biomass (represented by the particulate fraction, POP). The P cycling component simulated the exchange of P among the three pools by the processes of production and remineralization of organic matter. We then did a sensitivity analysis to evaluate how changes in the remineralization and distribution of particles could affect phytoplankton biomass.

405

400

The circulation model reproduced global patterns of mass transport for each fraction (Table S2). The circulation model was constrained using a data-assimilation technique that incorporated observations of several tracers^{36,37}. The model simulated transport of the two dissolved forms (DIP and DOP) using an advection and diffusion

410 operator T (T = $\nabla [U - k\nabla]$), which is a $N \times N$ sparse matrix (N: the number of wet grid boxes). T was constrained by multiple tracers including temperature, salinity, mean sea surface height, natural radiocarbon, CFC-11, air-sea heat exchange and freshwater sources^{36,38}. Biomass is subject to sinking and remineralization as particulate organic matter in the water column following a power law function (i.e., Martin curve). The 415 exponential decay (b) was implicitly incorporated into a particle flux divergence operator (F in Eq. 10) and was optimized as part of the inversion (Table S2).

DIP losses were simulated as the phytoplankton uptake as well as transport, and DIP gains by remineralization and influx of deep water to the euphotic layer. DIP consumption rate was modeled using satellite-derived NPP together with two tunable parameters (// and //) (Eq. 9 and Table S2)³⁸.

$$\gamma = \alpha \frac{[NPP/R_{C:P}]^{\beta}}{[DIP]_{obs}} \tag{9}$$

 $\gamma = \alpha \frac{[NPP/R_{C:P}]^{\beta}}{[DIP]_{obs}} \tag{9}$ where the unit of NPP was converted to mmol C m⁻² s⁻¹, \square is a dimensionless parameter, and $R_{C:P}$ is the carbon to phosphate ratio. The assimilation rate (γ) had the same units as [](s⁻¹). Gains of DOP were simulated by DIP assimilation to organic matter and by POP dissolution, and losses were simulated by DOP remineralization. Gains of POP were simulated by DIP assimilation and losses by POP dissolution. Changes in the three components of P cycle are summarized in Eq. 13.

$$\left[\frac{d}{dt} + \mathbf{T}\right] [DIP] = -\gamma [DIP] + \kappa_d [DOP] + \kappa_g ([DIP] - [\overline{DIP}]_{obs}),$$

$$\left[\frac{d}{dt} + \mathbf{T}\right] [DOP] = \sigma \gamma [DIP] + \kappa_p [POP] - \kappa_d [DOP],$$

$$\left[\frac{d}{dt} + \mathbf{F}\right] [POP] = (1 - \sigma) \gamma [DIP] - \kappa_p [POP],$$
(10)

420

425

435

440

445

where $[\overline{\text{DIP}}]$ is volume weighted average DIP concentration, κ_g is a geological restore term, which is a small value (i.e., $1/10^{-6}$ yr) and is used to restored DIP concentration to observed global mean; σ is a parameter that governed the partition of DIP assimilation in production of DOP and POP. We used $\sigma = 1/3$, which means that one third of DIP is produced as DOP and the rest as POP (Eq. 10). κ_d is the DOP remineralization rate optimized as part of the inversion (Table S2). Finally, κ_p is the POP dissolution rate and is set at $\kappa_p = 1/30 \text{ day}^{-1}$.

Most ocean biogeochemical concepts and models include a direct or implied control of nutrient supply on upper ocean biomass. Thus, we used the model to explore three possible alternative mechanisms for regulation of upper ocean biomass and manipulated values within their known range. The first mechanism is based on the principle that increased temperature leads to smaller surface phytoplankton (like *Prochlorococcus*) with lower sinking speed leading to remineralization closer to the surface. To simulate this effect, we modified b in the range of $\pm 15\%$. The second mechanism is that increase temperature leads to higher remineralization of DOP to DIP. To simulate this effect, we modified κ_d in the range of +/- 15%. The third mechanism is that the C:P ratio of phytoplankton is higher in a warmer, nutrient deplete future ocean environment^{28,39,40}. To simulate this effect, we compare biomass levels using C:P based

- on Redfield proportions (106:1) vs. the empirical relationship determined by Galbraith and Martiny³⁹. Finally, we tested the effect of a change with a combination of all mechanisms.
- Acknowledgments. We thank the many contributing researchers for the oceanographic data and Katherine Mackey and Jennifer Martiny at UCI for helpful comments. Financial support for this work was provided by the National Science Foundation (OCE-1046297 and OCE-1848576 to ACM), CONICET, UBACYT (20020170100620BA), and Agencia Nacional de Promoción Científica y Tecnológica (PICT-2017-3020 to PF) and US Department of Energy Office of Biological and Environmental Research (DE-SC0012550 to FP).

Author contributions. PF and ACM designed the study. PF, WW and FP did the analysis, and ACM wrote the paper.

465 **References:**

- 1. Bopp, L. *et al.* Multiple stressors of ocean ecosystems in the 21st century: Projections with CMIP5 models. *Biogeosciences* **10**, 6225–6245 (2013).
- 2. Cabre, A., Marinov, I. & Leung, S. Consistent global responses of marine ecosystems to future climate change across the IPCC AR5 earth system models. *Clim. Dyn.* **45**, 1253–1280 (2015).
- 3. Bienfang, P. K., Szyper, J. P., Okamoto, M. Y. & Noda, E. K. Temporal and spatial variability of phytoplankton in a subtropical environment. *Limnol. Oceanogr.* **29**, 527–539 (1984).
- 4. Moon-van der Staay, S. Y., De Wachter, R. & Vaulot, D. Oceanic 18S rDNA sequences from picoplankton reveal unsuspected eukaryotic diversity. *Nature* **409**, 607–610 (2001).
 - 5. Irwin, A. J., Nelles, A. M. & Finkel, Z. V. Phytoplankton niches estimated from field data. *Limnology and Oceanography* **57,** 787–797 (2012).
- 6. Flombaum, P. *et al.* Present and future global distributions of the marine Cyanobacteria *Prochlorococcus* and *Synechococcus. Proc. Natl. Acad. Sci. U. S. A.* **110,** 9824–9829 (2013).
 - 7. Hoegh-Guldberg, O. & Bruno, J. F. The Impact of Climate Change on the World's Marine Ecosystems. *Science* (80-.). **328**, 1523–1528 (2010).
- 8. Moore, J. K. *et al.* Sustained climate warming drives declining marine biological productivity. *Science* (80-.). **359**, 1139–1143 (2018).
 - 9. Graff, J. R. *et al.* Photoacclimation of natural phytoplankton communities. *Mar. Ecol. Prog. Ser.* **542,** 51–62 (2016).
 - 10. McQuatters-Gollop, A. *et al.* Is there a decline in marine phytoplankton? *Nature* (2011). doi:10.1038/nature09950
- 490 11. Quéré, C. Le *et al.* Ecosystem dynamics based on plankton functional types for

- global ocean biogeochemistry models. Glob. Chang. Biol. 11, 2016–2040 (2005).
- 12. Lomas, M. W., Bonachela, J. A., Levin, S. A. & Martiny, A. C. Impact of ocean phytoplankton diversity on phosphate uptake. *Proc. Natl. Acad. Sci.* **111**, 17540–17545 (2014).
- 495 13. Rusch, D. B. *et al.* The Sorcerer II Global Ocean Sampling Expedition: Northwest Atlantic through Eastern Tropical Pacific. *PLoS Biol.* **5**, e77 (2007).
 - 14. Irwin, A. J., Finkel, Z. V, Müller-Karger, F. E. & Troccoli Ghinaglia, L. Phytoplankton adapt to changing ocean environments. *Proc. Natl. Acad. Sci.* **112**, 5762–5766 (2015).
- Larkin, A. A. & Martiny, A. C. Microdiversity shapes the traits, niche space, and biogeography of microbial taxa. *Environ. Microbiol. Rep.* **9,** 55–70 (2017).
 - 16. Colwell, R. K. & Rangel, T. F. Hutchinson's duality: The once and future niche. *Proc. Natl. Acad. Sci.* **106**, 19651–19658 (2009).
- 17. Li, W. K. W. From cytometry to macroecology: A quarter century quest in microbial oceanography. *Aquat. Microb. Ecol.* **57**, 239–251 (2009).
 - 18. Morán, X. A. G., López-Urrutia, Á., Calvo-Díaz, A. & LI, W. K. W. Increasing importance of small phytoplankton in a warmer ocean. *Glob. Chang. Biol.* **16**, 1137–1144 (2010).
- Landry, M. R., Kirshtein, J. & Constantinou, J. Abundances and distributions of picoplankton populations in the central equatorial Pacific from 12 degrees N to 12 degrees S, 140 degrees W. *Deep. Res. Part Ii-Topical Stud. Oceanogr.* 43, 871–890 (1996).
 - 20. Rodríguez, F. *et al.* Ecotype diversity in the marine picoeukaryote *Ostreococcus* (Chlorophyta, Prasinophyceae). *Environ. Microbiol.* **7,** 853–9 (2005).
- 515 21. Six, C. *et al.* Contrasting photoacclimation costs in ecotypes of the marine eukaryotic picoplankter *Ostreococcus*. *Limnol. Oceanogr.* **53**, 255–265 (2008).

- 22. Moore, L. R., Goericke, R. & Chisholm, S. W. Comparative physiology of *Synechococcus* and *Prochlorococcus*: influence of light and temperature on growth, pigments, fluorescence and absorptive properties. *Mar. Ecol. Prog. Ser.* 116, 259–275 (1995).
- 23. Kulk, G., De Vries, P., Van De Poll, W. H., Visser, R. J. W. & Buma, A. G. J. Temperature-dependent growth and photophysiology of prokaryotic and eukaryotic oceanic picophytoplankton. *Mar. Ecol. Prog. Ser.* **466**, 43–55 (2012).
- Buitenhuis, E. T. *et al.* Picophytoplankton biomass distribution in the global ocean. *Earth Syst. Sci. Data* **4,** 37–46 (2012).
 - 25. Rivkin, R. B. & Legendre, L. Biogenic carbon cycling in the upper ocean: effects of microbial respiration. *Science* **291**, 2398–2400 (2001).
 - 26. Rafter, P. A., Sigman, D. M. & Mackey, K. R. M. Recycled iron fuels new production in the eastern equatorial Pacific Ocean. *Nat. Commun.* **8,** 1100 (2017).

- White, A. E., Watkins-Brandt, K. S., Engle, M. A., Burkhardt, B. & Paytan, A. Characterization of the rate and temperature sensitivities of bacterial remineralization of dissolved organic phosphorus compounds by natural populations. *Front. Microbiol.* **3**, (2012).
- Martiny, A. C. *et al.* Strong latitudinal patterns in the elemental ratios of marine plankton and organic matter. *Nat. Geosci.* **6,** 279–283 (2013).
 - 29. Martiny, A. C., Vrugt, J. A., Primeau, F. W. & Lomas, M. W. Regional variation in the particulate organic carbon to nitrogen ratio in the surface ocean. *Global Biogeochem. Cycles* **27**, 723–731 (2013).
- 30. Moreno, A. R. & Martiny, A. C. Ecological Stoichiometry of Ocean Plankton. *Ann. Rev. Mar. Sci.* **10,** 43–69 (2018).
 - 31. Morel, A. *et al.* Examining the consistency of products derived from various ocean color sensors in open ocean (Case 1) waters in the perspective of a multi-sensor approach. *Remote Sens. Environ.* **111**, 69–88 (2007).
- 32. Casey, J. R., Aucan, J. P., Goldberg, S. R. & Lomas, M. W. Changes in partitioning of carbon amongst photosynthetic pico- and nano-plankton groups in the Sargasso Sea in response to changes in the North Atlantic Oscillation. *Deep. Res. Part II Top. Stud. Oceanogr.* **93**, 58–70 (2013).

- 33. Dunne, J. P. *et al.* GFDL's ESM2 global coupled climate-carbon earth system models. Part II: Carbon system formulation and baseline simulation characteristics. *J. Clim.* **26**, 2247–2267 (2013).
 - 34. Taylor, K. E., Stouffer, R. J. & Meehl, G. A. An overview of CMIP5 and the experiment design. *Bulletin of the American Meteorological Society* **93**, 485–498 (2012).
- Pearman, P. B., Guisan, A., Broennimann, O. & Randin, C. F. Niche dynamics in space and time. *Trends in Ecology and Evolution* **23**, 149–158 (2008).
 - 36. DeVries, T. & Primeau, F. Dynamically and Observationally Constrained Estimates of Water-Mass Distributions and Ages in the Global Ocean. *J. Phys. Oceanogr.* **41**, 2381–2401 (2011).
- Primeau, F. W., Holzer, M. & DeVries, T. Southern Ocean nutrient trapping and the efficiency of the biological pump. *J. Geophys. Res. Ocean.* **118,** 2547–2564 (2013).
 - 38. Teng, Y.-C., Primeau, F. W., Moore, J. K., Lomas, M. W. & Martiny, A. C. Global-scale variations of the ratios of carbon to phosphorus in exported marine organic matter. *Nat. Geosci.* **7**, 895–898 (2014).
- 565 39. Galbraith, E. D. & Martiny, A. C. A simple nutrient-dependence mechanism for predicting the stoichiometry of marine ecosystems. *Proc. Natl. Acad. Sci. U. S. A.* 112, 8199–8204 (2015).
 - 40. Yvon-Durocher, G., Dossena, M., Trimmer, M., Woodward, G. & Allen, A. P. Temperature and the biogeography of algal stoichiometry. *Glob. Ecol. Biogeogr.*